Systems/Circuits

The Organization of Prefrontal-Subthalamic Inputs in Primates Provides an Anatomical Substrate for Both Functional Specificity and Integration: Implications for Basal Ganglia Models and Deep Brain Stimulation

William I. A. Haynes[1,2] **and Suzanne N. Haber**[1]

[1]Department of Pharmacology and Physiology, University of Rochester School of Medicine and Dentistry, Rochester, New York 14642 and [2]Centre de Recherche de l'Institut du Cerveau et de la Moelle Epiniere (CRICM), Inserm U 975, CNRS 7225, UPMC, 75013 Paris, France

The identification of a hyperdirect cortico-subthalamic nucleus connection highlighted the important role of the subthalamic nucleus (STN) in regulating behavior. However, this pathway was shown primarily from motor areas. Hyperdirect pathways associated with cognitive and motivational cortical regions are particularly relevant given recent data from deep brain stimulation, both for neurologic and psychiatric disorders. Our experiments were designed to demonstrate the existence and organization of prefrontal-STN projections, help delineate the "limbic" STN, and determine whether convergence between cortico-STN fibers from functionally diverse cortical areas exists in the STN. We injected anterograde tracers in the ventromedial prefrontal, orbitofrontal, anterior cingulate, and dorsal prefrontal cortices of *Macaca nemestrina* and *Macaca fascicularis* to analyze the organization of terminals and passing fibers in the STN.

Results show a topographically organized prefrontal hyperdirect pathway in primates. Limbic areas project to the medial tip of the nucleus, straddling its border and extending into the lateral hypothalamus. Associative areas project to the medial half, motor areas to the lateral half. Limbic projections terminated primarily rostrally and motor projections more caudally. The extension of limbic projections into the lateral hypothalamus, suggests that this region be included in the STN. A high degree of convergence exists between projections from functionally diverse cortical areas, creating potentially important interfaces between terminal fields. Taken together, the results provide an anatomical substrate to extend the role of the hyperdirect pathway in models of basal ganglia function, and new keys for understanding deep brain stimulation effects on cognitive and motivational aspects of behavior.

Introduction

The subthalamic nucleus (STN), once considered as a relay nucleus of the basal ganglia involved in inhibiting unwanted motor programs (Mink, 1996), is now also known to regulate cognition, motivation, and impulsivity (Kuhn et al., 2005; Eagle and Baunez, 2010; Huebl et al., 2011). Pallidal projections support a tripartite STN organization comprising a dorsolateral motor area, a central associative region, and a ventromedial limbic component (Haber et al., 1993; Shink et al., 1996; Karachi et al., 2005). The demonstration of direct motor and premotor cortical inputs (hyperdirect pathway) (Nambu et al., 1996) coupled with its pallidal input from the indirect pathway first suggested that the STN was involved in the temporal bounding of motor programs (Nambu et al., 2002). The hyperdirect pathway is currently thought to exert top-down executive control over all behavioral programs transiting through the basal ganglia, by establishing decisional thresholds (Bogacz and Larsen, 2011; Cavanagh et al., 2011). This complex function probably involves direct inputs from multiple frontal regions. Although motor and premotor cortices terminate in a large lateral portion of the STN and caudal prefrontal areas terminate medial to those (Künzle, 1976; Hartmann-von Monakow et al., 1978; Nambu et al., 1996), little is known about the projections from rostral and ventral prefrontal areas. Given the importance of the hyperdirect pathway in filtering behavioral output, including cognition and emotion, our first goal was to delineate the terminal organization of all prefrontal inputs to the STN, distinguishing them from the related passing fibers.

With the development of STN deep brain stimulation (DBS) for obsessive-compulsive disorder (OCD) (Mallet et al., 2008) and possibly addiction (Luigjes et al., 2012), which targets the medial STN, a clearer definition of the STN areas associated with emotion and motivation is crucial. Early descriptions of the STN boundaries point out the difficulty in delineating a clear medial border (Luys, 1865; Dejerine, 1901). The separation between

Received Aug. 21, 2012; revised Dec. 17, 2012; accepted Jan. 16, 2013.

Author contributions: W.I.A.H. and S.N.H. designed research; W.I.A.H. and S.N.H. performed research; W.I.A.H. and S.N.H. analyzed data; W.I.A.H. and S.N.H. wrote the paper.

This work was supported by National Institute of Mental Health Grants MH 045573, MH 086500, and MH045573. W.I.A.H. received a doctoral grant from the French Ministry for Higher Education and Research through the University Paris Descartes (Paris, France). We thank Rebecca Finelli, Julia Lehman, and Anna Borkowska-Belanger for technical assistance.

S.N.H. received speaker honorarium from Pfizer and Medtronic.

Correspondence should be addressed to Suzanne N. Haber, Department of Pharmacology and Physiology, University of Rochester School of Medicine and Dentistry, 601 Elmwood Avenue, Rochester, NY 14642. E-mail: Suzanne_haber@urmc.rochester.edu.

DOI:10.1523/JNEUROSCI.4674-12.2013

 0270-6474/13/334804-11$15.00/0

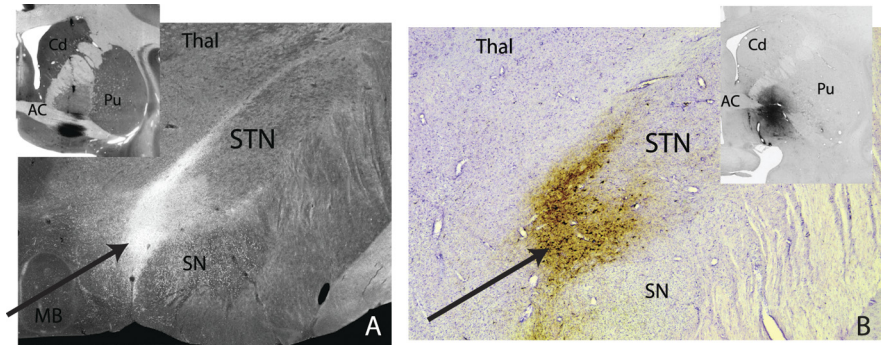

Figure 1. Ventral pallidal connections to the STN. ***A***, Coronal section illustrating VP terminal fields at the edge of the medial STN border, extending medially into the hypothalamus following an injection in the subcommissural ventral pallidum (inset). ***B***, A coronal section illustrating labeled cells (and terminals) at the edge of the medial STN border, extending medially into the hypothalamus after an injection that includes the ventral pallidum. AC, Anterior commissure; Cd, caudate nucleus; MB, mammillary body; Pu, putamen; SN, substantia nigra; STN, subthalamic nucleus; Thal, thalamus.

STN and lateral hypothalamus (LH) is obscure, considering both cytoarchitectonics (Dejerine, 1901) and ventral pallidal (VP) connections (Fig. 1) (Haber et al., 1993). Therefore, our second goal was to use ventromedial PFC (vmPFC), orbitofrontal (OFC), and dorsal anterior cingulate (dACC) afferent projections to help delineate the "limbic" STN.

Convergence between cortical terminals from functionally diverse areas exists in both the striatum and thalamus (McFarland and Haber, 2002; Haber et al., 2006). Consistent with the possibility of a similar pattern of convergence in the hyperdirect pathway, DBS for Parkinson's disease shows a variation in non-motor responses despite electrode locations centered in the dorsal motor region (Mallet et al., 2007; Hershey et al., 2010). Our third goal was to determine whether there is also convergence of cortico-STN fibers from functionally diverse cortical areas.

Our results show both a functional topography and a convergence of cortico-STN projections from different functional regions, and support the idea that the lateral LH may be considered as part of the limbic STN. Finally, passing fibers from each functional region travel widely through the STN. These data impact the functional models of STN and DBS approaches in neurology and psychiatry.

Materials and Methods

To examine the organization of frontal cortico-subthalamic projections, we injected anterograde and bidirectional tracers into different frontal cortical regions. Corticocortical, corticostriatal, and corticothalamic labeling was used to verify the specificity of the injection sites. We charted the entire projection field and passing fibers throughout the STN in each case. In addition to the traditional charting of individual terminating fibers, we outlined dense projection fields for each case to create 3D maps of these dense fields. These maps were then compiled to delineate the entire subthalamic region that receives its primary input from each of the frontal areas that was injected. A 3D map combining all the dense projection fields and fibers outside of those fields (diffuse projections) was created to determine the extent of a possible interaction between different frontal cortex regions.

Surgery and tissue preparation. Forty-three adult male macaque monkeys (4 *Macaca nemestrina*, 39 *Macaca fascicularis*) were used for the tracing study. All experiments were conducted in accordance with the *Guide for the Care and Use of Laboratory Animals* (National Research Council, 1996) and were approved by The University Committee on Animal Resources.

Monkeys were tranquilized by intramuscular injection of ketamine (10 mg/kg). A surgical plane of anesthesia was maintained by intravenous injections of pentobarbital (initial dose of 20 mg/kg, i.v., and maintained as needed). Temperature, heart rate, and respiration were monitored throughout the surgery. Monkeys were placed in a David Kopf Instruments stereotactic frame, a midline scalp incision was made, and the muscle and fascia were displaced laterally to expose the skull. A craniotomy (~2-3 cm^2) was made over the region of interest, and small dural incisions were made only at injection sites. To guide deep cortical injections, serial electrode penetrations were made to locate fiber tracts as indicated by absence of cellular activity (Haber et al., 1993) (i.e., corpus callosum and anterior commissure). We calculated the anterior/posterior position of various prefrontal regions based on the location of the anterior commissure. Accurate placement of tracer injections was achieved by careful alignment of the injection cannulas with the electrode. In several animals, we obtained magnetic resonance images to guide our injection sites. The dorsolateral injections sites were determined by visual inspection of frontal cortical gyri, indicating general frontal cortical areas.

Monkeys received an injection of one or more of the following anterograde/bidirectional tracers: Lucifer yellow (LY), fluororuby (FR), or fluorescein (FS) conjugated to dextran amine [40–50 nl, 10% in 0.1 M phosphate buffer (PB), pH 7.4; Invitrogen], or tritiated amino acids (100 nl, 1:1 solution of [3H]-leucine and [3H]-proline in dH_2O, 200 mCi/ml; NEN). Tracers were pressure injected >10 min using a 0.5 μl Hamilton syringe. After each injection, the syringe remained *in situ* for 20 to 30 min. Twelve to 14 days after the operation, monkeys were again deeply anesthetized and perfused intracardially with saline, followed by a 4% paraformaldehyde/1.5% sucrose solution in 0.1 M phosphate buffer, pH 7.4. Brains were postfixed overnight and cryoprotected in increasing gradients of sucrose (10, 20, and 30%). Serial sections of 50 μm were cut on a freezing microtome into 0.1 M phosphate buffer or cryoprotectant solution as previously described (Haber et al., 2000).

Immunocytochemistry. Immunocytochemistry was performed on free-floating sections (1 in 8 for each tracer) to visualize LY, FR, and FS tracers. Before incubation in primary antisera, tissue was treated with 10% methanol and 3% hydrogen peroxide in 0.1 PB to inhibit endogenous peroxidase activity and rinsed 1 to 2 h in PB with 0.3% Triton X-100 (TX) (Sigma). Sections were preincubated in 10% normal goat serum (NGS) and 0.3% TX in PB for 30 min. Tissue was placed in the primary anti-LY (1:3000 dilution; Invitrogen), anti-FS (1:1000; Invitrogen), anti-FR (1:1000; Invitrogen) in 10% NGS, and 0.3% TX in PB for 4 nights at 4°C. After extensive rinsing, the tissue was incubated in biotinylated secondary antibody, followed by incubation with the avidin–biotin complex solution (Vectastain ABC kit; Vector Laboratories). Immunoreactivity was visualized using standard DAB procedures. Staining was intensified by incubating the tissue for 5 to 15 min in a solution of 0.05% 3,3′-diaminobenzidine tetra-hydrochloride (DAB), 0.025% cobalt chloride, 0.02% nickel ammonium sulfate, and 0.01% H_2O_2 to yield a black reaction product. Sections were mounted onto gel-coated slides, dehydrated, defatted in xylenes, and coverslipped with Permount. In cases in which more than one tracer was injected into a single animal, adjacent sections were processed for each antibody reaction. To visualize amino acid staining, sections were mounted on chrome-alum gelatin-subbed slides for autoradiography. Sections were defatted in xylene for 1 h, and then dipped in Kodak NTB 2 photographic emulsion. Exposure time of the autoradiograms ranged from 6 to 9 weeks. The sections were then developed in Kodak D for 2.5 min, fixed, washed, and counterstained with cresyl violet.

Data analysis. A total of 48 injections were placed throughout the frontal cortex. Five of the 43 monkeys had 2 tracer injections, each in a different part of cortex. We focused on prefrontal cortex; however, we also included a few motor and premotor cases for comparison purposes. Specifically targeted prefrontal areas were as follows: the vmPFC (areas 14, 25, and ventral 32), the OFC (areas 11, 13, 12, and orbital proisocor-

tex), the dACC (area 24), the DPFC (areas 10, 9, and 46). Motor regions included area 6 and medial M1 (area 4). Five animals received two injections into different regions of the frontal cortex.

Cortical injections with contamination or weak labeling were eliminated from the analysis (16 cases). Contamination refers to all injections in which the tracer was not limited to a single cortical region but had leaked into an adjacent area or into the underlying white matter. Weak labeling refers to relatively few labeled fibers in the thalamus, indicating that little if any would be transported to the STN. This was typically the result of injection sites centered in superficial cortical layers. Eleven cases that had injection sites in which there were other outstanding cases were not fully charted. These cases were used to validate those cases that were fully charted and modeled. Thus, a total of 21 injection sites were charted and modeled.

All thin, labeled fibers containing boutons were charted for LY, FR, and FS injections. Areas where those fibers formed clusters sufficiently dense to be visualized at low magnification (4×) were labeled as dense terminal fields and were outlined as distinct objects. Terminating fibers outside of these dense areas were also charted, but were considered to form a diffuse projection system (Haber et al., 2006). Thick fibers without clear terminal boutons were assumed to be passing fibers and were charted separately. Fiber distribution for each case was charted throughout the rostrocaudal extent of the STN. For cases with tritiated amino acid injections, only the dense terminal fields were charted. Indeed, diffuse projections could not be distinguished from passing fibers due to the lack of morphological identification of individual fibers.

3D reconstruction. The 3D reconstructions of focal and diffuse projection fields in the STN were developed to (1) address how each projection lies within the STN space and (2) study a possible convergence of the different inputs. For each case, a stack of 2D coronal sections was created from its Neurolucida chartings and Nissl images. This stack was imported into IMOD, a 3D rendering program (Boulder Laboratory for 3D Electron Microscopy of Cells, University of Colorado, Boulder, CO) (Kremer et al., 1996), and a 3D reconstruction that contained the dense and diffuse projections was created for each case separately. To merge several cases together, we developed a reference model of the STN from one animal. This model was created by sampling 1 in 8 sections (at 400-μm intervals) throughout the STN, using alternate high resolution photographs of frozen sections, taken as they were cut, and Nissl-stained sections. Data from each case was then transposed into the reference STN using landmarks of key internal structures (anterior commissure, caudate nucleus, putamen, midline, mammillary bodies, internal globus pallidus, substantia nigra, optic tract). After the transposition of dense and diffuse projections from each case, every contour placed in the reference model was checked with the original for medial/lateral, dorsal/ventral, and anterior/posterior placement and relative size. This ensured that the dense projection field from each case was accurately placed with respect to its position and the proportion of the STN it occupied. Thus, a 3D rendering was created first for each single case and then for the combination of cases.

Results

We charted the subthalamic projections resulting from 21 injections. Two injections were located in area 14, 1 in area 11/13, 1 in area 12 orbital proisocortex, 3 in area 24, 1 in area 10, 3 in area 9, 2 in area 46, 4 in area 6, and 4 in medial area 4. All injection sites were confined, covering a relatively small portion of each cortical area. Tracer uptake and axonal transport varied across cases, thereby influencing the amount and density of labeling in the STN. Therefore, we did not attempt to correlate injection location to projection volumes and density. In addition, we found that, in general, the more rostral injections resulted in less transport compared with injections closer to the STN. This was evident not only in the STN but in thalamic labeling as well. Therefore, we concluded that distance might affect the robustness of the terminal field. Nonetheless, although the density may vary between each case in this manner, the center of the projection area for each cortical region was consistent.

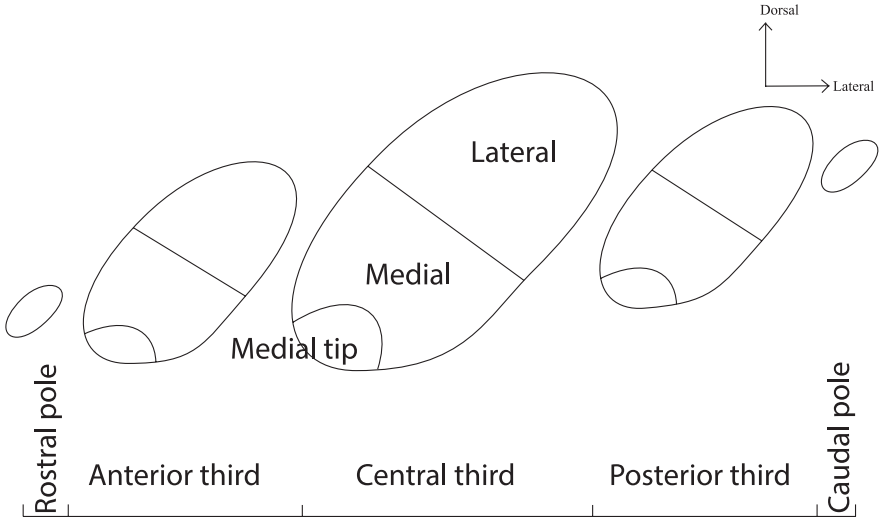

Figure 2. Schematic of the STN divisions. The STN was divided into thirds along the rostrocaudal axis, the rostral and caudal poles were considered as additional, distinct entities as they had specific properties. The medial tip also had specific properties and was isolated from the medial half.

For analysis, we divided the STN into thirds along the rostrocaudal axis (anterior third, central third, posterior third). In addition, we isolated the rostral and caudal poles because they had specific characteristics. Three medial-lateral divisions were used: medial and lateral halves, and the medial tip. The medial tip was also isolated from the rest of the medial half as it appeared to have a different organization (Fig. 2). We selected one representative case of each region for illustration purposes.

Overall, descending cortical fibers traveled to the STN through the internal capsule (IC). Caudal to the anterior commissure, fiber bundles from each cortical region split into two bundles (Lehman et al., 2011): one branch sent fibers to the thalamus, the other to the brainstem. Axons branched off from the brainstem portion of the IC at different rostrocaudal levels to enter the STN. The level at which fibers split off from the IC depended on the cortical region they originated from.

vmPFC/OFC

Axons from the vmPFC/OFC traveled ventral to, or within the anterior commissure and thus within the most ventral portion of the IC (Lehman et al., 2011). Although these fibers entered the STN through the ventromedial aspect of the anterior third, they mainly coursed along the medial tip, in the lateral hypothalamus (LH). Overall, there were few terminals within the STN's conventional borders. Indeed, the majority of vmPFC terminal fields were located medially to the medial tip of the STN, in the general area of the LH (Fig. 3*A*). Diffuse terminals surrounded the dense projection fields and extended into the medial STN. Those from the OFC surrounded the medial tip of the STN, also straddling its border (Fig. 3*B*). This organization was seen primarily in the anterior third of the nucleus. We observed few terminals in the

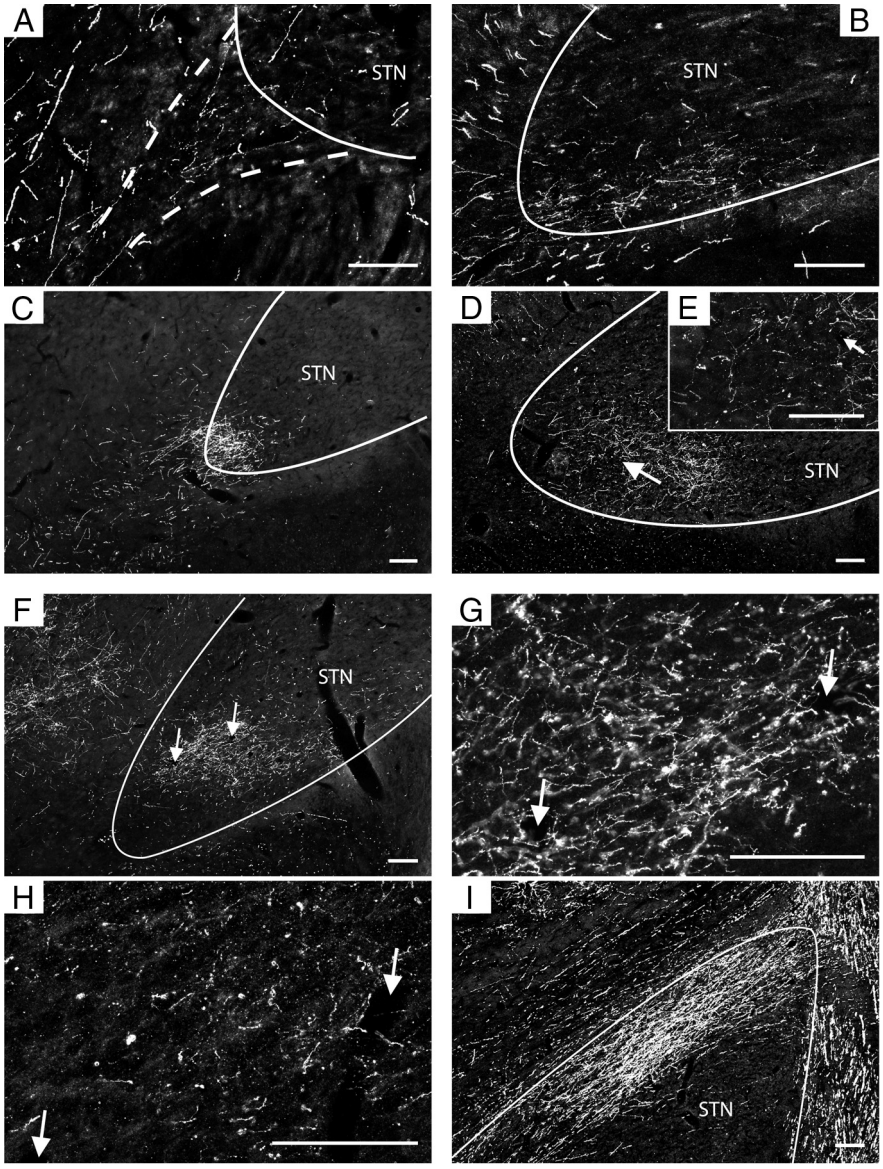

Figure 3. Photomicrographs of STN labeling after cortical injections of anterograde tracers (dark field microscopy of coronal sections). ***A***, Projections from OFC are mostly located medial to the STN's conventional boundaries (solid white line), but are contained within the STN's limits according to Dejerine (dashed white lines). ***B***, Projections from vmPFC straddle the conventional medial boundary of the STN (white line). ***C***, The dense projection from dACC is concentrated in the medial tip of the STN and is in a position to overlap with the vmPFC projection (***B***). It also extends beyond the medial boundary, creating a potential interface with OFC projections (***A***). ***D***, The projection from area 9 is located in the medial half of the STN. Although the dense projection does not occupy the medial tip, diffuse projections do, providing an interface with dACC (***C***). This is visible in ***E***, a micrograph from the same case at a higher magnification (the white arrows in ***D*** and ***E*** indicate the same blood vessel). ***F***, Projections from the rostral area 6 are more caudal and somewhat more dorsal than DPFC projections. Nonetheless, DPFC and area 6 projections overlap extensively. This is demonstrated in ***G*** the same section as ***F*** at a higher magnification, and in ***H*** the section adjacent to ***F*** and ***G***, showing the result of a DPFC injection in the same monkey. Matching blood vessels in ***F–H*** are indicated by the white arrows. Lesser intensity of staining in ***H*** is likely the result of variations in transport (see Results). ***I***, Projections from M1 are dorsal and lateral. Scale bars, 200 μm.

central and posterior thirds (Fig. 4*A*). OFC and vmPFC terminal fields overlapped extensively, and therefore we combined their distributions in Figure 3*A*.

dACC

Three injections were placed at different rostrocaudal positions in area 24. One was located in the most rostral part of area 24, the second was immediately anterior to the genu of the corpus callosum, and the third was in the caudal part of area 24, above the genu (but rostral to the midcingulate cortex). dACC fibers traveling to the STN were located dorsal to those from the vmPFC/OFC in the IC. Fibers left the brainstem component of the IC just rostral to the STN and were in a position to enter the nucleus through the center of its rostral pole. Thereafter, they traveled primarily in the medial tip, extending into the medial half. In addition, some passing fibers traveled in the lateral half.

dACC fibers terminated throughout the rostral pole, with the exception of its most lateral aspect. In the anterior and central thirds, fibers collected into a dense projection field that was located in the medial tip. Part of this field extended outside the STN's medial boundary into the LH, partially overlapping with those from the vmPFC/OFC (compare Figs. 3*A–C*). Diffuse terminals surrounded this terminal field, occupying the medial half of the STN and also extending outside of the conventional boundaries, into the adjacent LH. The dense projection did not extend into the posterior third of the STN. Indeed, the number of diffuse terminating fibers decreased steadily in the caudal sections. Those that did extend posteriorly were confined to a small area in the medial tip of the STN, as well as outside of the medial border (Fig. 4*B*).

DPFC

Descending fibers from all DPFC injection sites traveled in the IC dorsally to the fibers from the ventral prefrontal regions. These fibers traveled in the IC with the brainstem axons until the anterior pole of the STN. Unlike dACC axons that entered the rostral pole of the STN centrally, DPFC axons entered the rostral pole from its lateral aspect. However, the axons then crossed to the medial half of the STN, where the terminal fields were concentrated. A few passing fibers remained in the lateral half and some could also be seen in the medial tip.

In the anterior third, the main terminal field from area 10 was confined to the dorsal portion of the medial half. The surrounding diffuse terminals occupied most of the anterior third and extended to the rostral pole and ventromedial part of the central third. There were few terminals in the rostral pole or in the posterior third. Diffuse terminals from area 9 occupied the medial half of the anterior third, with the notable exception of the medial tip. In the central third, the dense projection field from area 9 was located ventromedially, overlapping with the diffuse projections from area 10, but somewhat lateral to the dense terminals from the dACC injections (Figs. 3*D*, 4*C*). As with projections from the dACC, diffuse terminals from area 9 were scattered in the medial tip of the posterior third and no terminals were seen

Figure 4. Charts of frontal projections to the STN. Three coronal sections, evenly spaced along the rostrocaudal axis, are illustrated in the left panel of the figure to indicate the approximate anterior (AP = 11.10), central (AP = 10.2), and posterior thirds (AP = 9.0) levels depicted for each case (***A–G***). Scale bar, 5 mm. The schematic for the injection sites illustrate the center of the injection. Photographs of the prefrontal injection sites complement the prefrontal cases schematics to illustrate the extent of the halo around the injection sites. ***A***, Projections from the vmPFC/OFC (red) are mainly outside of the conventional medial borders of the STN, and concentrated in the anterior third. ***B***, Projections from the dACC (orange) are concentrated in the medial tip of the STN and extend over its medial border. ***C***, ***D***, Projections from DPFC (areas 9 and 46, respectively) (yellow) lie in the medial half of the STN, dorsal and lateral to projections from dACC (***B***). ***E***, Projections from the rostral area 6 (green) appear caudally to other PFC projections, lateral but overlapping with area 46 dense projections (***D***). ***F***, Projections from caudal area 6 (green) are located in the ventrolateral STN. ***G***, Projections from M1 (blue) occupy the dorsolateral STN and seem to overlap primarily with caudal area 6 dense projections. Scale bar: (left, bottom) ***A–G***, 1 mm. SN, Substantia nigra; STN, subthalamic nucleus; ZI, zona incerta.

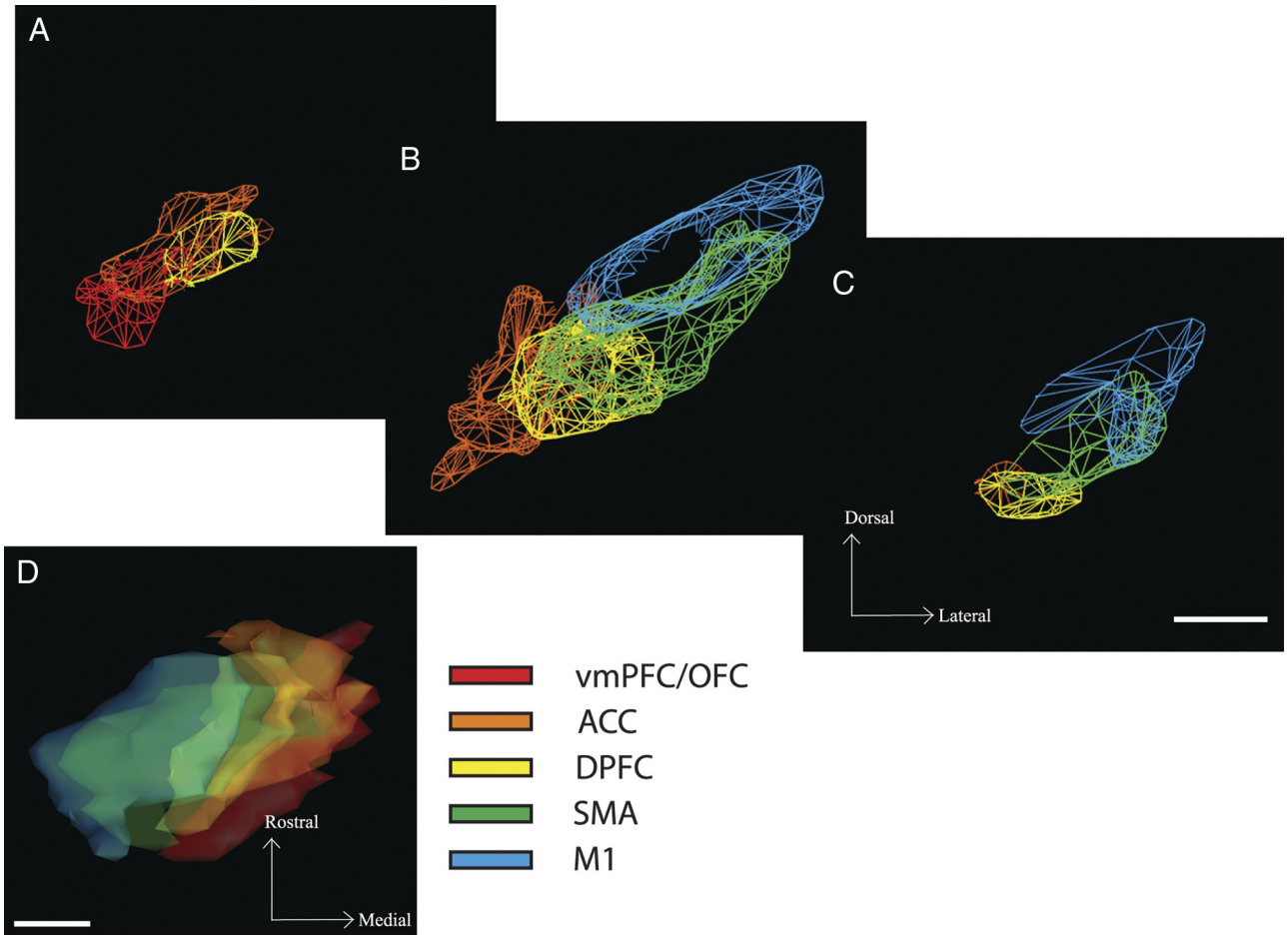

Figure 5. Overlap of dense projections. ***A–C***, Coronal view at anterior (***A***), central (***B***), and posterior (***C***) thirds of the 3D model. Approximate AP levels are similar to those in Fig. 3. Colored meshes represent the outer surface of the combined dense projections from each cortical area. Overlaps occur mainly between projections from functionally close cortical regions. ***D***, Axial, superior view of the same dense projections. Scale bar, 1 mm.

in the caudal pole (Fig. 4*C*). Consistent with area 10 and area 9 projections, diffuse terminals from area 46 were also scattered throughout the anterior pole of the STN. There was a dense projection in the center of the anterior third. In the central third, this dense projection was somewhat dorsal to that from area 9. Unlike the other DPFC projections, this terminal field continued throughout the posterior third of the STN and diffuse terminals were observed in the caudal pole (Fig. 4*D*).

Motor areas

In contrast to PFC terminals that entered at the rostral pole, descending fibers from area 6 and M1 entered the STN through the dorsolateral aspect of the anterior and central thirds respectively. Whereas area 6 axons then descended to occupy the medial and lateral halves of the STN (rostral and caudal area 6, respectively), M1 axons remained in the dorsolateral portion. Neither area 6 nor M1 injections gave rise to terminals in the rostral pole of the STN. Area 6 diffuse terminals occupied the dorsal half of the anterior third, where there were few from PFC areas. In the central and posterior thirds, there was rostrocaudal topography to area 6 inputs. Rostral area 6 projected ventrally in the medial half, somewhat lateral to, but overlapping area 46 projections (Figs. 3*F*, 4*E*). The caudal area 6 projected to the lateral half, caudal and lateral to PFC projections (Fig. 4*F*). Surrounding these dense projections, diffuse fibers were scattered throughout the STN, avoiding the medial tip of the STN in the anterior and central thirds. In contrast to area 6, terminals from M1 occupied a dorsal position in the lateral half of the STN, throughout its rostrocaudal extent. The projection was most dense in the central third (Fig. 3*I*). There were a small dense projection and some diffuse terminals in the center of the caudal pole (Fig. 4*G*).

General topography

Taken together, cortico-subthalamic projections defined a functional, rostral to caudal, ventromedial to dorsolateral topography within the STN. The anterior third of the STN contained primarily PFC dense terminal fields. dACC dense projections straddled the medial tip, while combined DPFC dense projections occupied the medial half of the nucleus. The central third contained dense projections from the entire frontal cortex. dACC dense terminal fields remained in the medial tip, DPFC projections occupied the medial STN, whereas M1 dense projections were concentrated dorsal in the lateral half, and area 6 terminals took a more central location, between DPFC and M1 projections. The posterior third contained primarily motor projections, with M1 dense terminal fields occupying the center of the nucleus, whereas rostral and caudal area 6 dense terminal fields extended in a gradient from the medial tip to the M1 dense projection. The remainder of the DPFC terminal fields was confined to the medial tip at this level (Fig. 5).

In addition to projections within the conventional boundaries of the STN, dACC terminals in the anterior and central thirds of

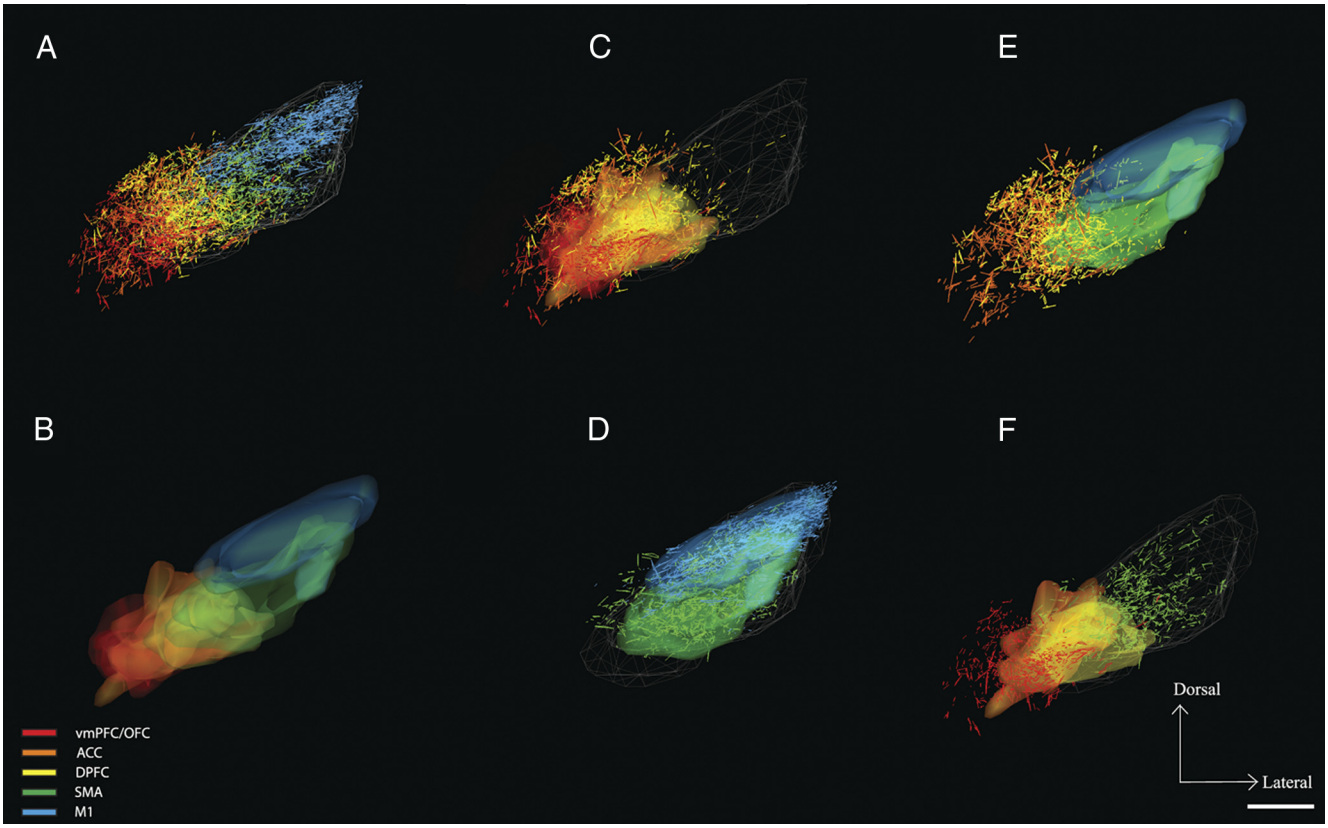

Figure 6. Overlap of diffuse projections. Posterior, coronal 3D views of diffuse and dense cortical projections. Colored volumes/surfaces, Dense projection fields; colored lines, diffuse projections. ***A***, All diffuse projections. The topography is the same as for dense projections, although there is more overlap. ***B***, All dense projections (surfaces). Note, compared to the diffuse projections in ***A***, the dense terminal fields show less overlap. ***C***, Diffuse and dense projections from prefrontal areas, vmPFC, ACC, and DPFC. Diffuse projections increase the interface between the different prefrontal inputs. ***D***, Diffuse and dense projections from premotor and motor regions. ***E***, Diffuse projections derived from DPFC and dACC injections extend into area 6 and M1 territory, thus increasing their interface. ***F***, Reciprocally, area 6 diffuse projections extend into the prefrontal projection territory. They are also able to interface with diffuse projections from vmPFC/OFC. Scale bar, 1 mm.

the STN, and DPFC terminals in the posterior third, straddled the medial boundaries to extend into the adjacent LH. This projection pattern established a topographic continuity with the vmPFC/OFC dense terminal fields that were concentrated outside of the conventional STN boundaries, along its medial tip, but located within the LH (Fig. 5).

Topology

The OFC/vmPFC projected to an area overlapping with terminals from the medial component of the dACC dense projection (those lying within the LH; Figs. 3*A–C*, 5*A*,*B*). While medial dACC terminals overlapped with those from the vmPFC/OFC in the LH, its dense projection system was primarily located within the conventional boundary of the STN. The lateral part of the terminal field overlapped with inputs from the DPFC (Figs. 3*C–E*, 5*A*,*B*). These lateral dACC projections also overlapped, but to a much lesser extent, with rostral area 6 projections (Fig. 5*B*). The lateral DPFC fibers terminated in the same area as those from the rostral area 6 (Figs. 3*F–H*, 5*B*). Finally, the dorsal portion of the area 6 dense projection field also received inputs from M1 (Fig. 5*B*,*C*).

Diffuse projections (Fig. 6*A*), although centered on their respective dense projections (Fig. 6*B*), extended over a greater territory. Thus, despite a relatively conserved medial to lateral and rostral to caudal organization (Fig. 6*A*), diffuse projection fields from each area overlapped much more extensively than their dense counterparts (Fig. 6*C*,*D*). This topology allowed extended interfaces between prefrontal (dACC, DPFC) and motor regions (Fig. 6*E*). Moreover, motor diffuse projections also extended into the medial, prefrontal territories of the STN (Fig. 6*F*). The most striking example of this extended convergence is the DPFC projection, of which the dense component primarily converged with the dACC and area 6 dense projections, whereas its diffuse projections interfaced with the projections from all frontal areas. The diffuse projections increased the convergence both between different prefrontal projections (Fig. 6*C*), as well as between premotor and motor projections (Fig. 6*D*).

Overall, the different functional territories, although topographically organized, were not completely segregated. This topology showed two types of overlap. The first type was the convergence between dense terminal fields from different frontal regions (Figs. 5, 6*B*). This occurred primarily, but not entirely, between projections from neighboring cortical regions (e.g., vmPFC and dACC, dACC and DPFC). The second type involved the wider spread of diffuse fibers, allowing an overlap from functionally more distant cortical areas (e.g., DPFC and M1) (Fig. 6).

Passing fibers also followed this topology (Fig. 7*A*). vmPFC/OFC fibers were located primarily medial to the medial tip and dACC fibers within the medial tip, extending partly through the medial half (Fig. 7*B*). The DPFC axons traveled primarily in the medial half, but also in the medial tip and the lateral half (Fig. 7*C*). The rostral area 6 axons traveled in the medial half in a similar region as those from the DPFC. However, these rostral area 6 axons were positioned more laterally. Thus, they also intermingled with the axons from the caudal area 6. Passing fibers from M1 were concentrated in the lateral half and did not travel

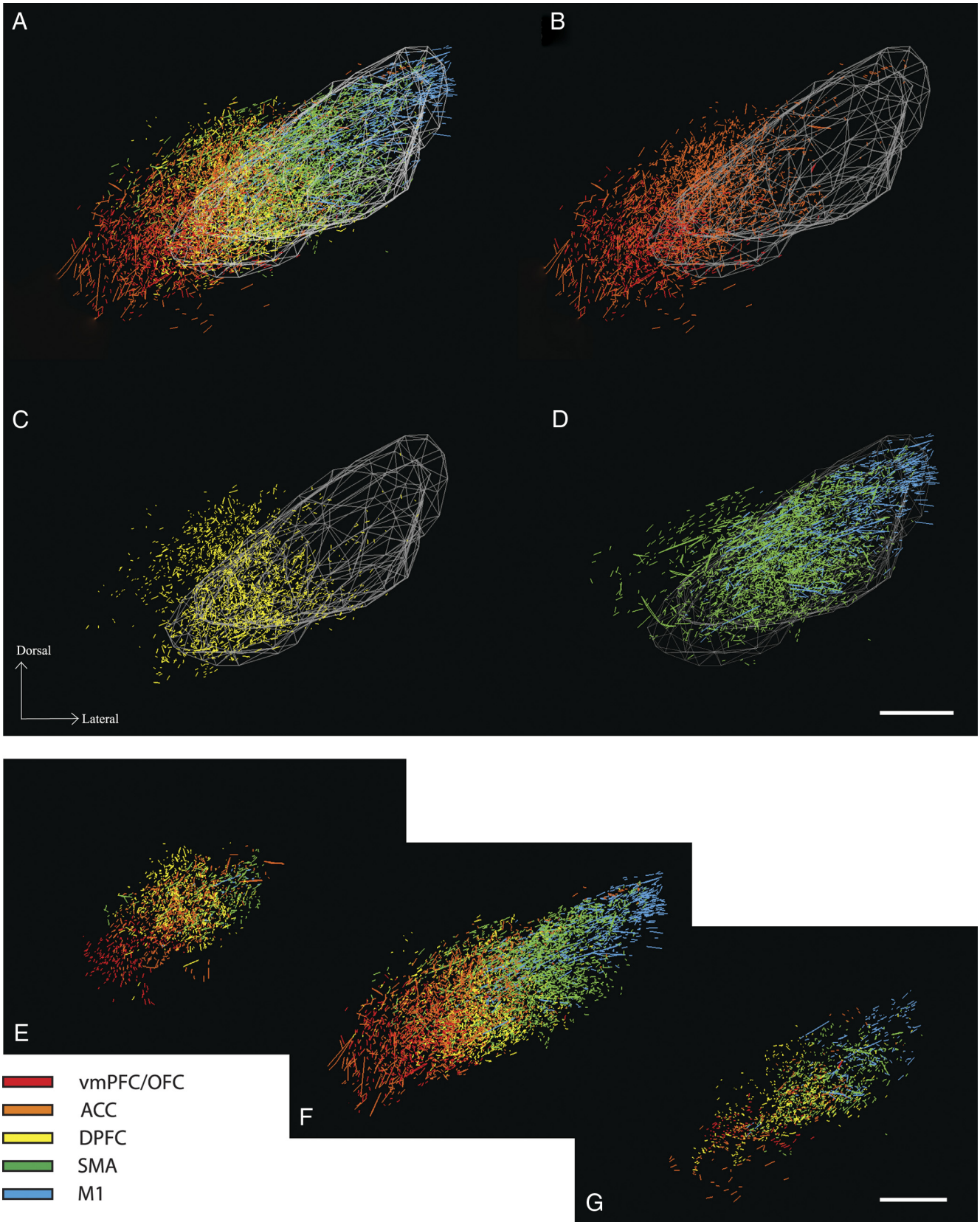

Figure 7. Passing fibers. ***A***, Passing fibers have a topographic organization similar to diffuse projections (Fig. 6*A*). ***B***, Fibers from vmPFC, OFC, and dACC travel in the medial tip of the STN and in the adjacent lateral hypothalamus. ***C***, Fibers from DPFC travel in the medial half of the STN. ***D***, Fibers from rostral and caudal area 6 travel, respectively, in the medial and lateral halves of the STN. Fibers from M1 travel in the dorsal portion of the lateral half. ***E–G***, Views of the anterior, central, and posterior thirds of the STN illustrate the rostrocaudal topography of passing fibers. Prefrontal fibers enter the STN rostrally (***E***) to those from area 6 and M1 (***F***). However, fibers from area 6 and M1 travel further caudally (***G***). Scale bar, 1 mm.

through the medial half (Fig. 7*D*). The rostrocaudal organization of passing fibers is illustrated in Figure 7*E–G*.

Discussion

General topography

All prefrontal areas project to or within the immediate region of the STN, following a general functional topography. Prefrontal projections are concentrated in the anterior, ventral, and medial half of the STN. dACC dense terminal fields are located in the anterior, medial tip, an area previously described as devoid of cortical inputs (Hartmann-von Monakow et al., 1978). DPFC projections occupy the medial half of the STN. Consistent with the literature, we found that M1 projects to the dorsolateral STN and the area 6 projects ventromedially to M1 projections (Kunzle and Akert, 1977; Hartmann-von Monakow et al., 1978; Nambu et al., 1996, 1997). Importantly, our injections did not sample the entire frontal cortex and injection sites were small. Therefore, the projection fields of each region may be larger than what we report here.

The limbic STN

One important finding is the location of the terminals from vmPFC/OFC and dACC. Whereas DPFC dense projections are contained within the conventional medial border of the STN, dACC projections straddle this border and vmPFC/OFC terminals are located outside of it in the adjacent LH. Thus, the cone-shaped region that surrounds the ventromedial tip of the STN and is occupied by vmPFC/OFC and part of the dACC projections contains elements of the STN. Indeed, the cortical terminal fields in this area are in the topographic continuity of the other PFC projections. Moreover, terminals from, and cells to the VP, a known subthalamic input/output, are in the same location surrounding the medial tip of the STN (Fig. 1*B*,*C*) (Haber et al., 1993). Finally, these terminal fields are contained within the area that extends to the mammillary bodies which has been historically attributed to the STN based on cytoarchitectonics (Dejerine, 1901), but is not functionally well characterized.

The cognitive STN

Previous experiments reported STN terminals from areas 8, caudal 46, and caudal 9 (Hartmann-von Monakow et al., 1978). As described here, these were located ventral and medial to premotor and motor projections, but left the medial half of the STN free of cortical afferences. It is in this area that the projections from the more rostral injections located in areas 10, 9, and 46 terminate. The dACC, a cognitive and limbic structure, projects to the medial tip. Overlap between these different prefrontal projections is extensive, which suggests complex integration between the different cognitive inputs to the STN.

Overall, the hyperdirect pathway defines a topographic anatomic connection, composed of a rostral limbic component, concentrated in the medial tip of the STN and the adjacent LH, a cognitive component in the medial half, and a more lateral and caudal motor component, centered in the lateral half of the STN. This is consistent with the topography of the pallido-subthalamic interconnection (Haber et al., 1993; Shink et al., 1996; Karachi et al., 2005).

Physiological experiments support this organization. In monkeys, targeted pharmacological inactivations of the posterolateral STN induce contralateral ballistic movements, whereas anteromedial inactivations induce stereotyped and/or violent behavior (Karachi et al., 2009). In patients, DBS of the STN can induce a range of effects depending on the exact stimulation locus (Mallet et al., 2007; Hershey et al., 2010). Dorsal and lateral contacts induce pure motor manifestations, whereas stimulation with the more centrally located contacts provoke attentional issues, and stimulation at the ventral and medial contacts lead to manic symptoms (Mallet et al., 2007). Accordingly, the STN has become a target for DBS in resistant OCD, at a location rostral and medial to the one used for Parkinson's disease (Mallet et al., 2008). It is also a potential target for the treatment of severe addictions (Luigjes et al., 2012).

Topology: convergence and integration

OFC and vmPFC terminals overlap with dACC dense terminals in the medial tip of the STN and the LH. dACC converges with DPFC. DPFC terminals also overlap with those from area 6. M1 dense terminals overlap primarily with area 6 dense terminals. The motor region appears to be relatively isolated from the other functional regions. However, the range of our motor injection sites was limited and previous results suggest that M1 projections might extend further into the ventrolateral STN, providing a greater degree of overlap with area 6 projections (Nambu et al., 1996, 1997).

The length and orientation of the STN dendrites indicate that convergence between STN cortical inputs from different functional areas may be greater than it appears based on projection patterns. STN dendrites are oriented along the long axis of the nucleus and occupy approximately two-thirds of its volume (Yelnik and Percheron, 1979). Therefore, each dendrite stretches across multiple functional regions and receives inputs along its entire length. Inputs from the VP and globus pallidus have been shown to converge onto a single STN neuron (Bevan et al., 1997). Thus, STN neurons at the interface of functional territories are likely to receive convergent inputs onto their proximal dendrites. In addition, STN neurons at the center of a functional region may also receive inputs from functionally diverse cortical areas onto more distal dendrites (Bevan et al., 1997). Therefore, the output from each subthalamic neuron, although primarily driven by the cortical input matching the territory in which the neuron lies, is likely to result from the integration of functionally diverse information.

Functional considerations

The STN is thought to integrate contextual information through the hyperdirect pathway to set a decisional threshold. It is considered a filter that selects behavioral programs carried along the direct pathway. In other words, whereas potential behavioral programs pass through the striato-pallidal connection, the STN sends a signal to the internal globus pallidus that is driven by a direct cortical input. This signal arrives before that conveyed through the direct pathway (Nambu et al., 2002), allowing only the most appropriate program to be passed onto the thalamus. This functional construct is not limited to complex motor plans, but also includes perceptual decisions, making the assumption of a direct input from not only the caudal but also the rostral DPFC (Frank et al., 2007; Bogacz and Larsen, 2011). Our data demonstrate projections from throughout the DPFC (areas 10, 9, and 46). Moreover, we show that the vmPFC/OFC and dACC also contribute to the hyperdirect pathway. These findings extend the model to include more abstract cognitive and emotional selections. In addition, the convergence between terminals provides the anatomic substrate for the integration of emotional, motivational, and cognitive information toward the selection of complex behaviors. Of particular interest is that part of the LH is thought to integrate interoceptive, gustatory, olfactory, and nociceptive perceptions to regulate limbic behaviors (Berthoud and

Munzberg, 2011). This is consistent with the anatomic continuity between the STN and the LH: both regions appear to integrate contextual information to filter behavior, reinforcing the idea that a component of the LH might be considered as the limbic cone of the STN.

Implications for DBS

The delineation of limbic and cognitive hyperdirect pathways contributes to our understanding of non-motor effects of DBS in Parkinson's disease (PD) and as an experimental site for the treatment of OCD. Modeling studies indicate that, with the common clinical parameters, axons likely to be stimulated at the STN sites are within relative close proximity to the electrode, with large myelinated fibers being activated at greater distances from the electrode compared to those terminating (Chaturvedi et al., 2010). Here, we have shown that both terminating and passing fibers follow a functional topography, supporting the range of effects observed for different stimulation loci. However, axons passing through the stimulated area can originate from different functional regions and stimulation will affect these also. In addition, passing fibers (likely myelinated) will be sensitive to activation at a greater distance from the electrodes compared to terminating fibers. Taken together, stimulation of passing fibers from different cortical areas traveling through a given STN region coupled with the wider effective area of these axons indicates that stimulation likely impacts on cortical axons from adjacent functional regions. This may underlie nonmotor side effects seen in DBS for PD.

The presence of prefrontal STN inputs provides a more direct explanation of modifications in prefrontal activities observed after DBS in OCD (Le Jeune et al., 2010; Swann et al., 2011). DBS is thought to disrupt the pathological flow of information between motor cortex and STN caused by increased beta oscillations in PD (Kuhn et al., 2008). This explanation can now be extended to prefrontal areas and OCD, in which abnormal alpha oscillations have been found in the dACC and the STN (Koprivova et al., 2011; Welter et al., 2011), the subthalamic oscillations being predictive of DBS efficacy (Welter et al., 2011).

Taken together, our results demonstrate a topographic organization of prefrontal and motor inputs to the STN. However, this topography is not strict and the convergence we observed provides an additional anatomical substrate to integrated decision-making in the basal ganglia. In addition, the organization of passing fibers from the frontal cortex brings new anatomical elements to models of DBS mechanisms.

References

Berthoud HR, Münzberg H (2011) The lateral hypothalamus as integrator of metabolic and environmental needs: from electrical self-stimulation to opto-genetics. Physiol Behav 104:29–39. CrossRef Medline

Bevan MD, Clarke NP, Bolam JP (1997) Synaptic integration of functionally diverse pallidal information in the entopeduncular nucleus and subthalamic nucleus in the rat. J Neurosci 17:308–324. Medline

Bogacz R, Larsen T (2011) Integration of reinforcement learning and optimal decision-making theories of the basal ganglia. Neural computation 23:817–851. CrossRef Medline

Cavanagh JF, Wiecki TV, Cohen MX, Figueroa CM, Samanta J, Sherman SJ, Frank MJ (2011) Subthalamic nucleus stimulation reverses mediofrontal influence over decision threshold. Nat Neurosci 14:1462–1467. CrossRef Medline

Chaturvedi A, Butson CR, Lempka SF, Cooper SE, McIntyre CC (2010) Patient-specific models of deep brain stimulation: influence of field model complexity on neural activation predictions. Brain stimulation 3:65–67. CrossRef Medline

Dejerine J (1901) Anatomie des centres nerveux. Paris: Rueff.

Eagle DM, Baunez C (2010) Is there an inhibitory-response-control system in the rat? Evidence from anatomical and pharmacological studies of behavioral inhibition. Neurosci Biobehav Rev 34:50–72. CrossRef Medline

Frank MJ, Samanta J, Moustafa AA, Sherman SJ (2007) Hold your horses: impulsivity, deep brain stimulation, and medication in parkinsonism. Science 318:1309–1312. CrossRef Medline

Haber SN, Lynd-Balta E, Mitchell SJ (1993) The organization of the descending ventral pallidal projections in the monkey. J Comp Neurol 329:111–128. CrossRef Medline

Haber SN, Fudge JL, McFarland NR (2000) Striatonigrostriatal pathways in primates form an ascending spiral from the shell to the dorsolateral striatum. J Neurosci 20:2369–2382. Medline

Haber SN, Kim KS, Mailly P, Calzavara R (2006) Reward-related cortical inputs define a large striatal region in primates that interface with associative cortical inputs, providing a substrate for incentive-based learning. J Neurosci 26:8368–8376. CrossRef Medline

Hartmann-von Monakow K, Akert K, Künzle H (1978) Projections of the precentral motor cortex and other cortical areas of the frontal lobe to the subthalamic nucleus in the monkey. Exp Brain Res 33:395–403. Medline

Hershey T, Campbell MC, Videen TO, Lugar HM, Weaver PM, Hartlein J, Karimi M, Tabbal SD, Perlmutter JS (2010) Mapping Go-No-Go performance within the subthalamic nucleus region. Brain 133:3625–3634. CrossRef Medline

Huebl J, Schoenecker T, Siegert S, Brücke C, Schneider GH, Kupsch A, Yarrow K, Kühn AA (2011) Modulation of subthalamic alpha activity to emotional stimuli correlates with depressive symptoms in Parkinson's disease. Mov Disord 26:477–483. CrossRef Medline

National Research Council (1996) Guide for the care and use of laboratory animals. Washington, DC: National Academies Press.

Karachi C, Yelnik J, Tandé D, Tremblay L, Hirsch EC, Francois C (2005) The pallidosubthalamic projection: an anatomical substrate for nonmotor functions of the subthalamic nucleus in primates. Mov Disord 20:172–180. CrossRef Medline

Karachi C, Grabli D, Baup N, Mounayar S, Tandé D, Francois C, Hirsch EC (2009) Dysfunction of the subthalamic nucleus induces behavioral and movement disorders in monkeys. Mov Disord 24:1183–1192. CrossRef Medline

Koprivova J, Congedo M, Horacek J, Prasko J, Raszka M, Brunovsky M, Kohutova B, Hoschl C (2011) EEG source analysis in obsessive-compulsive disorder. Clin Neurophysiol 122:1735–1743. CrossRef Medline

Kremer JR, Mastronarde DN, McIntosh JR (1996) Computer visualization of three-dimensional image data using IMOD. J Struct Biol 116:71–76. CrossRef Medline

Kühn AA, Hariz MI, Silberstein P, Tisch S, Kupsch A, Schneider GH, Limousin-Dowsey P, Yarrow K, Brown P (2005) Activation of the subthalamic region during emotional processing in Parkinson disease. Neurology 65:707–713. CrossRef Medline

Kühn AA, Kempf F, Brücke C, Gaynor Doyle L, Martinez-Torres I, Pogosyan A, Trottenberg T, Kupsch A, Schneider GH, Hariz MI, Vandenberghe W, Nuttin B, Brown P (2008) High-frequency stimulation of the subthalamic nucleus suppresses oscillatory beta activity in patients with Parkinson's disease in parallel with improvement in motor performance. J Neurosci 28:6165–6173. CrossRef Medline

Künzle H (1976) Thalamic projections from the precentral motor cortex in Macaca fascicularis. Brain Res 105:253–267. CrossRef Medline

Künzle H, Akert K (1977) Efferent connections of cortical, area 8 (frontal eye field) in Macaca fascicularis. A reinvestigation using the autoradiographic technique. J Comp Neurol 173:147–164. CrossRef Medline

Le Jeune F, et al. (2010) Decrease of prefrontal metabolism after subthalamic stimulation in obsessive-compulsive disorder: a positron emission tomography study. Biol Psychiatry 68:1016–1022. CrossRef Medline

Lehman JF, Greenberg BD, McIntyre CC, Rasmussen SA, Haber SN (2011) Rules ventral prefrontal cortical axons use to reach their targets: implications for diffusion tensor imaging tractography and deep brain stimulation for psychiatric illness. J Neurosci 31:10392–10402. CrossRef Medline

Luigjes J, van den Brink W, Feenstra M, van den Munckhof P, Schuurman PR, Schippers R, Mazaheri A, De Vries TJ, Denys D (2012) Deep brain stimulation in addiction: a review of potential brain targets. Mol Psychiatry 17:572–583. CrossRef Medline

Luys JB (1865) Recherches sur le système nerveux cérébro-spinal: sa structure, ses fonctions et ses maladies. Paris: J.-B. Baillière et Fils.

Mallet L, et al. (2008) Subthalamic nucleus stimulation in severe obsessive-compulsive disorder. N Engl J Med 359:2121–2134. CrossRef Medline

Mallet L, Schüpbach M, N'Diaye K, Remy P, Bardinet E, Czernecki V, Welter ML, Pelissolo A, Ruberg M, Agid Y, Yelnik J (2007) Stimulation of subterritories of the subthalamic nucleus reveals its role in the integration of the emotional and motor aspects of behavior. Proc Natl Acad Sci U S A 104:10661–10666. CrossRef Medline

McFarland NR, Haber SN (2002) Thalamic relay nuclei of the basal ganglia form both reciprocal and nonreciprocal cortical connections, linking multiple frontal cortical areas. J Neurosci 22:8117–8132. Medline

Mink JW (1996) The basal ganglia: focused selection and inhibition of competing motor programs. Prog Neurobiol 50:381–425. CrossRef Medline

Nambu A, Takada M, Inase M, Tokuno H (1996) Dual somatotopical representations in the primate subthalamic nucleus: evidence for ordered but reversed body-map transformations from the primary motor cortex and the supplimentary motor area. J Neurosci 16:2671–2683. Medline

Nambu A, Tokuno H, Inase M, Takada M (1997) Corticosubthalamic input zones from forelimb representations of the dorsal and ventral divisions of the premotor cortex in the macaque monkey: comparison with the input zones from the primary motor cortex and the supplementary motor area. Neurosci Lett 239:13–16. CrossRef Medline

Nambu A, Tokuno H, Takada M (2002) Functional significance of the cortico-subthalamo-pallidal 'hyperdirect' pathway. Neurosci Res 43:111–117. CrossRef Medline

Shink E, Bevan MD, Bolam JP, Smith Y (1996) The subthalamic nucleus and the external pallidum: two tightly interconnected structures that control the output of the basal ganglia in the monkey. Neuroscience 73:335–357. CrossRef Medline

Swann N, Poizner H, Houser M, Gould S, Greenhouse I, Cai W, Strunk J, George J, Aron AR (2011) Deep brain stimulation of the subthalamic nucleus alters the cortical profile of response inhibition in the beta frequency band: a scalp EEG study in Parkinson's disease. J Neurosci 31:5721–5729. CrossRef Medline

Welter ML, Burbaud P, Fernandez-Vidal S, Bardinet E, Coste J, Piallat B, Borg M, Besnard S, Sauleau P, Devaux B, Pidoux B, Chaynes P, Tézenas du Montcel S, Bastian A, Langbour N, Teillant A, Haynes W, Yelnik J, Karachi C, Mallet L (2011) Basal ganglia dysfunction in OCD: subthalamic neuronal activity correlates with symptoms severity and predicts high-frequency stimulation efficacy. Transl Psychiatry 1:e5. CrossRef Medline

Yelnik J, Percheron G (1979) Subthalamic neurons in primates: a quantitative and comparative analysis. Neuroscience 4:1717–1743. CrossRef Medline